The submitted manuscript has been authored by a contractor of the U.S. Government under Contract No. DE-AC05-00OR22725. Accordingly, the U.S. Government retains a nonexclusive royalty-free license to publish or reproduce the published form of this contribution, or allow others to do so, for U.S. Government purposes.

Anomalous diffusion and exit time distribution of particle tracers in plasma turbulence model*

B. A. Carreras and V. E. Lynch

Oak Ridge National Laboratory, Oak Ridge, Tennessee 37830, U.S.A.

G. M. Zaslavsky

Courant Institute of Mathematical Sciences, New York University,

New York, New York 10012 U. S. A.

and Physics Department, New York University, New York, New York 10013, U. S. A.

Abstract

To explore the character of transport in a plasma turbulence model with avalanche transport, we have followed the motion of tracer particles. Both the time evolution of the moments of the distribution function of the tracer particle radial positions, $\left\langle \left| r(t) - r(0) \right|^n \right\rangle$, and their finite scale Lyapunov number are used to determine the anomalous diffusion exponent, ν. The numerical results show that the transport mechanism is superdiffusive with an exponent ν close to 0.88 ± 0.07. The distribution of the exit times of particles trapped into stochastic jets is also determined. These particles have the lowest separation rate at the low resonant surfaces.

PAC: 52.35.Ra, 52.25.Fi, 52.25,Gj

---

* Research sponsored by the Office of Fusion Energy, U.S. Department of Energy, under contract DE-AC05-00OR22725 with UT-Battelle, LLC and Coop. Agreement DE-FC02-99ER54512.

1. Introduction

Some of the phenomena observed in plasmas confined by magnetic fields suggest that a broad range of space and timescales play an essential role in the dynamics of the plasma. In particular, transport of particles and energy induced by turbulence has features that are not explained by local diffusive transport models. Two of these features are the non-gyroBohm scaling of the energy confinement[1] and the anomalous plasma response measured in perturbative experiments.[2,3] One of the possible explanations[4] is that high-temperature magnetically confined plasmas are close to marginal stability and their dynamics are governed by self-organized criticality (SOC).[5]

The concept of SOC brings together the ideas of self-organization of nonlinear dynamical systems with the often-observed near-critical behavior of many natural phenomena.[6] These phenomena exhibit self-similarities over extended ranges of spatial and temporal scales. In such systems, a feature of the dynamics is the existence of transport events of all sizes that we usually denote as avalanches.

Results of the analysis of fluctuation data from several experiments, including tokamaks, stellarators, and reversed field pinch, showed the self-similar character of the electrostatic fluctuations with a Hurst exponent,[7] H, in the range 0.6 to 0.74.[8] It is well known that for a time series with $1 > H > 0.5$, the data has long-range time correlations and when $0.5 > H > 0$, the series has long-range anticorrelations. The absence of time correlations (i. e., random) gives $H = 0.5$. Therefore the plasma fluctuations show the presence of long-range time correlations. There is also evidence of radial correlations over distances longer than the correlation length of the fluctuations[9] and large structures has been directly observed in the plasma core temperature fluctuations.[10] Such a character of the plasma fluctuations is consistent with plasma transport by avalanches.

Three-dimensional (3-D) calculations of plasma turbulence based on different dynamical mechanisms have shown some of the characteristic SOC behavior[11,12] and the presence of radially elongated structures.[13] Some of the macroscopic results from these models when applied to subcritical conditions are consistent with results from simple

cellular automata calculations based on the dynamics of the sandpile.[4,14,15] In this simple model, transport processes are dominated by anomalous diffusion.[16]

To explore the character of the underlying transport in plasma turbulence, we have considered a 3-D pressure-gradient–driven turbulence model[11] that has already been used to identify the presence of avalanche transport. In this model, we have followed the motion of tracer particles. Several moments, $\langle |r(t) - r(0)|^n \rangle$, of the distribution of the particle radial locations have been determined and also their dependence on the elapsed time, $\langle |r(t) - r(0)|^n \rangle = D_0 t^{n\nu(n)}$. Because of the finite size of the system, we have also evaluated the finite scale Lyapunov number as an alternative technique to determine ν. Both methods agree in the value of ν. The determination of the exponent ν is important for constructing plasma transport models that incorporate the multiplicity of time scales involved in transport.

The calculated transport exponents may be explained in terms of fractional kinetics of the tracer particles,[17,18] and they can be related to the decay exponents of the trapping time distributions of these particles.

The rest of this paper is organized as follows. In Sec. 2, the turbulence model used in the present calculations is described. The results of the tracer particle transport are presented in Sec. 3. In Sec. 4, we provide an interpretation of the numerical results in terms of fractional kinetics. Finally, the conclusions of this paper are given in Sec. 5.

2. Turbulence Model

We start with a cylindrical plasma confined by a magnetic field with average bad curvature. This plasma can be unstable to resistive interchange modes. The dissipative terms control the instability threshold and once they are included, the model is a critical gradient model. A typical example of this type of plasma is the outer region of a stellarator with magnetic shear. In the past, the resistive pressure-gradient-driven turbulence has been used to describe these plasmas in a supercritical state. The same basic model has been used in Ref. 11 to study a subcritical state. This model was

described in detail in Ref. 11. Here, we just summarize the basic equations. The fluctuation equations are as follows:

$$\frac{\partial \nabla^2\tilde{\Phi}}{\partial t} + \langle V_\theta \rangle \frac{1}{r}\frac{\partial \nabla^2\tilde{\Phi}}{\partial \theta} + \tilde{\vec{V}}\cdot\vec{\nabla}\nabla^2\tilde{\Phi} = -\frac{1}{\eta m_i n_0 R_0}\nabla_\parallel^2\tilde{\Phi} + \frac{B_0}{m_i n_0}\frac{1}{r_c}\frac{1}{r}\frac{\partial \tilde{p}}{\partial \theta} + \mu\nabla^4\tilde{\Phi}, \qquad (1)$$

$$\frac{\partial \tilde{p}}{\partial t} + \langle V_\theta \rangle \frac{1}{r}\frac{\partial \tilde{p}}{\partial \theta} + \tilde{\vec{V}}\cdot\vec{\nabla}\tilde{p} = \frac{\partial \langle p \rangle}{\partial r}\frac{1}{r}\frac{\partial \tilde{\Phi}}{\partial \theta} + \chi\nabla^2\tilde{p} + \chi_\parallel\nabla_\parallel^2\tilde{p}. \qquad (2)$$

Here, p and Φ are the pressure and electrostatic potential, the tildes indicate fluctuating quantities (in time and space), and the angular brackets, $\langle\ \rangle$, indicate flux surface averaging, that is, the poloidal and toroidal angular average. The cylinder has a radius a and length $2\pi R_0$. The magnetic field along the cylinder is B_0, the ion mass is m_i, the averaged radius of curvature of the magnetic field lines is r_c, and the resistivity is η. The total flow velocity is expressed in terms of an averaged poloidal velocity plus a fluctuating component given in terms of a stream function $\tilde{\Phi}/B_0$.

$$\vec{V} = \langle V_\theta \rangle \hat{\theta} + \left(\nabla\tilde{\Phi}\times\hat{z}\right)/B_0, \qquad (3)$$

where $\langle V_\theta \rangle$ is the poloidal flow velocity, which is a function only of t and r, and $\hat{\theta}$ and $\hat{z}$ are unit vectors in the poloidal and toroidal directions, respectively. The velocity stream function $\tilde{\Phi}/B_0$ is trivially related to the electrostatic potential $-\tilde{\Phi}$. In both Eqs. (1) and (2) there are dissipative terms with characteristic coefficients μ (the collisional viscosity) and χ (the collisional cross-field transport), respectively. A parallel dissipation term is also included in the pressure equation. This term can be interpreted as a parallel thermal diffusivity.

The instability drive is the flux surface averaged pressure gradient, $\partial\langle p \rangle/\partial r$, which is a function of r and t. The evolution equation of the flux surface averaged pressure is

$$\frac{\partial\langle p\rangle}{\partial t}+\frac{1}{r}\frac{\partial}{\partial r}r\left\langle\tilde{V}_r\tilde{p}\right\rangle=S_0+S_1+D\,\frac{1}{r}\frac{\partial}{\partial r}\left(r\frac{\partial\langle p\rangle}{\partial r}\right). \tag{4}$$

It contains a time-independent source term, S_0, which is only a function of r. This source of particles and heat is due, for instance, to neutral beam heating and fueling. In this case, S_0 is essentially determined by the beam deposition profile. In the present calculations, we use a parabolic profile, $S_0=\bar{S}_0\left[1-(r/a)^2\right]$. Even the best beams have time and radial variations in the amount of heating deposited; this is represented by an added noise term, S_1, which we choose to be random in radius and time. Implicitly, S_1 reflects variations on time scales slower than fluctuation time scales, of the order of $400\tau_{hp}$, hence its poloidal isotropy. Here, τ_{hp} is the poloidal Alfven time. The surface averaged quantities are not static, but they vary on time scales long compared to the fluctuations. The collisional diffusion coefficient, D, is taken to be different from the one in the fluctuation equation, Eq. (2).

The main transport mechanism that we study is the turbulent transport through the second term in the left-hand side of Eq. (4). However, the collisional diffusion term in the right-hand side is negligibly small for the calculations presented in this paper.

In a subcritical state, to reach a self-organized state (when such a state exists), it is necessary to have noise in the system. In some simple dynamical models, like the sandpile, the noise is external noise and the SOC state is reached by taking the limit of small noise. In the model presented here, there are two types of noise:

1. To start the 3-D nonlinear calculations, a low level of background fluctuations is initialized. These are the seeds for the instabilities to grow. We choose a random distribution of amplitudes and phases with an averaged fluctuation level below 10^{-5}. In our experience for fluctuation levels this low, the results in the nonlinear regime are not sensitive to these initial conditions.
2. The second source of noise is the external pressure source S_1 in Eq. (4). The external noise is not needed to reach a supercritical state. However, it is essential in exploring the subcritical regime.

3. Steady State Turbulence with Particle Tracers

To investigate the transport dynamics close to marginal stability, the model must have a critical pressure gradient below which resistive interchange modes are stable. This is achieved by having finite values of the dissipative terms in the fluctuation equations. These dissipative terms also control the width of the wavenumber spectrum. To be able to carry out these 3-D nonlinear calculations, we have to limit this width. Here, we take $\mu = 0.2\, a^2/\tau_R$ and $\chi = 0.025\, a^2/\tau_R$, where $\tau_R \equiv a^2\mu_0/\eta$ is the resistive time and a the minor radius. The resistivity is such that the Lundquist number is $S = 10^5$ for all these calculations, and $\beta_0/2\varepsilon^2 = 0.018$. Here, β_0 is the value of β at the magnetic axis and $\varepsilon = a/R_0$.

To avoid problems with the boundaries, only modes with resonant surfaces in the range $0.2 > r/a > 0.8$ have been included in the calculation. Outside this region, the collisional diffusivity D is increased by a factor of 4 to compensate for the lack of anomalous transport and to avoid distortion of the profiles. We include 363 Fourier components to represent the poloidal and toroidal angle dependence for each fluctuating component. The radial grid resolution is $\Delta r = 7.5 \times 10^{-4}\, a$. The nonlinear evolution has been carried out with the KITE code.[19]

To study the transport properties of this turbulence model, a steady state with a noise source, S_1, added must be reached. Here the assumption is that, in a time-averaged sense, the equilibrium pressure source maintains the averaged gradient. In general, however, this source is noisy. This noise is responsible for the dynamics in steady state. The noise is taken into account in the calculation as follows. At a fixed number of time steps (typically between 100 and 400), a small averaged pressure perturbation is added with a 50% probability. This addition of pressure corresponds to times of the order of $50\tau_{hp}$ to $200\tau_{hp}$. This perturbation is radially localized. It has a Gaussian form with a width of $W = 0.01\, a$; the amplitude is 0.05 times the local value of the normalized (to its $r = 0$ value) equilibrium pressure. The radial location of the averaged pressure perturbation is randomly chosen in the range $0 > r/a > 0.7$. A very low random level of non-

axisymmetric perturbations is also initialized (about 0.001% fluctuations) as a seed for the instabilities. We consider first the case without averaged poloidal velocity.

As the average pressure perturbations are added, they trigger local instabilities in the plasma at the corresponding resonance surface. The instability locally flattens the pressure profile and causes a change of gradient in the nearby surfaces, which may become unstable, and so continue the process. Eventually, the excess pressure deposited at the core is transported to the edge of the plasma. This process has the characteristic properties of an avalanche. It is a true avalanche in the sense that propagation is both up and down the gradient. The downward propagation is dominant. A more detailed description of the dynamics of this model is given in Ref. 11.

We use pseudo-particles as tracers because of the time requirements of the turbulence calculations. These tracers are solutions of the equation of motion:

$$\frac{d\vec{r}}{dt} = \vec{V}(\vec{r},t) \tag{5}$$

Here, the velocity is the $E\times B$ velocity because no diamagnetic effects are included in this model, and it is given in terms of the stream function

$$\vec{V}(\vec{r},t) = \frac{1}{B^2}\vec{E}\times\vec{B} = \frac{1}{B^2}\vec{\nabla}\Phi(\vec{r},t)\times\vec{B} \tag{6}$$

Because our model is electrostatic, all information on turbulence evolution is through Φ.

The tracers are initialized at random poloidal and toroidal positions around a given radius and with random initial velocities. Because in Eq. (6) the velocity component along the magnetic field is zero, the tracers move at a constant component of the velocity in this direction. This component is the initial one.

To investigate the dynamics of these tracer particles, we have followed their orbits. In their evolution, the tracer particles are either trapped in eddies for long times, or they can jump over several sets of eddies in a single flight (Fig. 1). Therefore, both characteristic features of the anomalous diffusion, particle trapping and particle flights,

are present in this model. Trapping times for tracer particles can be calculated, as it is described further down. However, from a quantitative point of view, there is no simple way of defining a flight.

The finite size of the system introduces practical problems in evaluating the dynamics of the tracers. These problems are particularly acute when there are such despair behavior on particle trajectories as the one illustrated in Fig. 1. In this situation, some particles stay trapped for very long times while other walk out of the system in very short times. A commonly used remedy[20,21] for dealing with the particles leaving the system is to put back into the plasma these tracer particles and keep following their orbits as if their radial positions are unbounded. This technique allows us to follow a bunch of tracer particles for as long as we desire, but it causes some distortions in the particle properties that we have to avoid as it will be discussed below.

In following the tracer orbits, we have calculated the ensemble average of several powers of the radial displacement as a function of time. As discussed in Ref. 16, because of the finite size of the system, it is useful to evaluate different moments of the distribution function of the radial positions of the tracer particle in order to extract the proper similarity exponent. That is, we calculate

$$\left\langle \left[r(t) - r(0) \right]^n \right\rangle = D_0 t^{n\nu(n)} , \tag{7}$$

where $r(t) \equiv |\vec{r}(t)|$. We evaluate Eq. (7) for different values of n, greater and smaller than 1. Here, the angular brackets indicate ensemble averaged over the particle tracers. From Eq. (7) we can, in principle, determine whether the diffusion is normal, $\nu = 0.5$, or anomalous, $\nu \neq 0.5$. Of course, if the probability distribution function of the particle positions at different times is not self-similar, the exponent ν can be a function of n. The consideration of several moments of the probability function allow us to determine its self-similarity properties.

In these studies, we have used 2000 tracer particles with random initial conditions around a given radial position. These particles are followed for two resistive times, that

is, 4×10^5 time steps. Over a time interval of about a decade, the moments of the tracer particle positions can be fitted by a power law. An example of the evaluated $n = 1$ and $n = 2$ moments is shown in Fig. 2. A power fit to the large t ($t > 0.1\ \tau_R$) power scaling region of these two moments gives $\nu = 0.91$ and $\nu = 0.84$, respectively. This is a clear indication that the transport is superdiffusive.

As discussed in Ref. 16 for the sandpile model, the probability distribution function (PDF) of the tracer particle positions at different times, $P(r, t)$, has different similarity scaling for large r and small r. This means that a simple scaling of the probability distribution of the form $P(r,t) = t^{-\nu} F\left(r/t^{\nu}\right)$ is not possible for all scales with the same value of ν. The self-similarity scaling is broken by the tracer particles that are put back into the plasma as a consequence of the finite size of the system. This symmetry breaking only affects the high-r region of the distribution. Therefore, to better determine ν, we calculate several moments of the distribution function as shown in Eq. (7) and determine $\nu(n)$. In Fig. 3, there is an example of the calculated $\nu(n)$. The figure shows that there are two linear scaling regions for $\nu(n)$, the low-n and high-n regions. They provide information on two regions of the PDF, for low r and high r, respectively. For high n, $\nu(n)$ is smaller than $\nu(n)$ for low n. For large n, $\nu(n)$ tends to be 0.5. For a particle moving in the plasma with position $r < a$, the flight length may be of the same size as the particle position. Therefore, this particle does not yet know that there is a limit in the size of a flight. When summing over flights, the distribution of sums is possibly close to a stable Levy distribution. However, when a tracer particle has moved out of the plasma and put back in several times, its effective radial position r is such that $r >> a$. Such a particle knows that the flights are all shorter than a. They have a Levy-like distribution that is truncated at a finite length. When partial sums of flights are done to calculate the particle motion, the particle positions no longer have a Levy-like distribution. Because of the truncation, the variance of the flights is finite, and the successive sums are distributed close to a Gaussian.[20] Therefore, the $n >> 1$ moments that sample these $r > L$ particle positions should scale with an index of $\nu \approx 0.5$. Note that the

$n > 1$ regime is only the result of the way we treat particles when they reach boundary. For low n, the value of ν is larger than 0.5. This is the relevant regime for the transport calculation because it describes the transport process within the minor radius of the plasma, that is for $r < a$. The values of $\nu(n)$ for all n's considered are plotted in Fig. 3. For $n < 2$, the averaged value is $\nu(n) = 0.81$, and $\nu(n) = 0.49$ for $n > 2$.

The separation of $\nu(n)$ in two regions allows us to calculate ν correcting for the problems introduced by the finite size of the system. However, it is never totally clear what is the proper time range for evaluating ν. As can be seen in Fig. 2, there are at least three regions in time where the moments defined in Eq. (8) can be fitted by a power law. We also know from the previous discussion, that if the calculation is taken further in time a non-physical diffusive region will ultimately appear. Is the last of the three regions in Fig. 2 the proper asymptotic region for this determination? This is a question difficult to answer with the available information. For this reason, we have applied an alternative approach[21] to determine the exponent ν.

When we determine the positions of the tracer particles at a given time, some of the particles can be quite far away from the bulk of the bunch, and some have even walked out of the system all together. Therefore, it makes sense in a finite size system to determine the time for a group of particles to reach a given distance. In this way, one has a better control of the particle positions. This is the essence of the method proposed in Ref. 21. Following this method, we define an initial mean square separation between a set of N particles as

$$\delta(0)^2 = \frac{1}{N}\sum_{i=1}^{N}\left| r_i(0)^2 - \langle r_i(0)\rangle^2 \right|, \tag{8}$$

where $\langle r_i(0)\rangle$ is the mean radial position of the tracer particle i,

$$\langle r_i(0)\rangle = \frac{1}{N}\sum_{i=1}^{N} r_i(0)\,. \tag{9}$$

We follow M bunches of N particles and determine for each bunch the time, $T_j(1)$, taken to multiply their initial mean square separation by a given factor ρ; that is, to have a mean square separation $\delta(1) = \rho\delta(0)$. The mean time to increase by a factor of ρ the mean separation between particles is then

$$\langle T_j(1)\rangle = \frac{1}{M}\sum_{j=1}^{M} T_j(1) \tag{10}$$

This experiment can be repeated by successive increases by a factor of ρ, the mean square separation between particles. After m iterations, the particles have a mean square separation of $\delta(m) = \rho^m\delta(0)$, and the average time taken to reach this state is $\langle T_j(m)\rangle$. This allows us to define a finite scale Lyapunov exponent:

$$\lambda[\delta(m)] \equiv \frac{\ln(\rho)}{\langle T_j(m)\rangle}. \tag{11}$$

Note that for $\delta \to 0$, Eq. (12) gives the Lyapunov exponent. In Fig. 4, and for the same plasma parameters and initial tracer particle positions as the calculation of Fig. 2, we have plotted the values of λ as a function of δ. As shown in this figure, λ as a function of δ has three very well defined regions. At very low values of δ, λ is independent of δ. In this region, λ is the Lyapunov exponent. The second region shows a power fall off,[21]

$$\lambda(\delta) \quad \delta^{-1/\nu}. \tag{12}$$

If the probability distribution function of the tracer particle positions is self-similar and as a consequence ν is independent of n, then from Eq. (7), we have $\delta \quad T^{\nu}$. From the definition of λ, Eq. (11), we can see that the exponent ν in Eq. (12) is the same ν as in Eq. (7); ν is the scaling exponent that we are seeking. In the third region, λ falls off very

fast. This last region corresponds to particles walking out of the system. In the present calculations, we have taken 15 bunches of 200 particles. A fit by a power law of the second region gives an exponent $\nu = 0.87 \pm 0.03$ for particles starting around $r = 0.3\,a$, and $\nu = 0.89 \pm 0.12$ for particles starting around $r = 0.5\,a$. These values are not inconsistent with the value determined by the first method $\nu = 0.81$.

In the case of supercritical transport, the noise source S_1 can be removed. We repeated the calculation of the particle tracers in this situation, and the plot of $\lambda(\delta)$ is shown in Fig. 5. A fit to the second algebraic region gives $\nu = 0.89 \pm 0.14$; this value is very close to the ones obtained for subcritical transport.

We can study the transport properties of this system from another perspective. Let us consider a particle trajectory that we call basic trajectory, and a second trajectory that starts simultaneously with the first one. The initial condition for the second trajectory differs from the basic one by a small distance δ_0. When the distance $\delta(t)$ between the two trajectories reaches a given value, δ_f , we measure and store the time T, such $\delta(T) = \delta_f$. At this point, we start a new trajectory for the same basic trajectory, and we repeat the process. After many iterations, we accumulate a sequence of times that it takes the trajectories to get δ_f apart. We also accumulate the information on the length along the orbit until the particles separate and on the radial position where they separate. This approach is similar to the usual method of determining the Lyapunov number, but for a finite size separation. In the following results, we have used $\delta_0 = 0.001a$, the lowest possible value, because of the limitation of the radial resolution, and $\delta_f = 0.003a$.

By looking at the PDF of the radial positions where the particles separate, we find that it has considerable structure. This structure is directly related to the rational values of the safety q profile. There are fewer events of particles separating at the radial position of a rational surface. At these positions where the turbulent eddies, are centered and within these eddies the particles are trapped for long times. These structures are the stochastic jets defined in Ref. 14, and they can be visualized as toroidal structures where the tracers are trapped and in which they travel along them at a relatively constant velocity. Between eddies or jets the trajectories become stochastic and the Lyapunov

number is large. In these regions, there are many particle separation events. We can see that in Fig. 6, where we have plotted PDF of the radial positions, where the particles separate. We have used a requirement of 100 events per bin to minimize noise; therefore, only structures associated with low rational surfaces remains. In the figure, we have also plotted the positions of these low rational surfaces.

A way of measuring the particle trapping times is by the time that the particles stay together in the stochastic jets. This is not necessarily an exact definition, but as it is seen in Fig. 6, it gives a good description of trapping times. The PDF of the trapping times provides additional information on transport properties of the tracer particles. As shown in Fig. 7, the PDF of the trapping times has a power tail for large values of the trapping times with a decay exponent –1.83 ± 0.22. If the system was unlimited, that would imply a divergence of the second moment of the PDF. The implications of this slow fall-off will be explored in the next section. As the tracer particle travel together, the length along the orbit before separation can also be calculated. As it is shown in Fig. 8, the PDF of the length along the trajectory decays as the –2.0 power for all values of the length. This may reflect that particle motion along the orbit is nearly uniform with the toroidal motion being the dominant one.

4. Fractional Kinetics of Particle Tracers

The information obtained from the tracer particles can be interpreted using the concept of fractional kinetics.[17,18] As mentioned in Sec. 1, large-scale fluctuations in the plasma take place and influence the tracer particle transport. We can identify the large-scale fluctuations with an appearance of spontaneous bursts in time-space dynamics or with coherent time-space structures (like “avalanches”). Tracers can be trapped in the vicinity of coherent structures and travel with the structure. This type of particle dynamics was called stochastic jets in Ref. 22. In our calculations, Fig. 6 shows the radial distribution of those jets. Particles in a jet are travelling together with other particles of the same jet. They have power law statistics of the particle's escape from the jet. Following this pattern, one can split the distribution function of tracers $P(x,t)$ into two parts, a normal P_n and singular P_s. It is the singular part of the distribution, $P_s(x,t)$,

that describes long-scale fluctuations and that is responsible for the anomalous diffusion. In one-dimensional (1-D) kinetics, $P_s(x,t)$ satisfies the fractional kinetic equation:

$$\frac{\partial^\beta P_s(x,t)}{\partial t^\beta} = D_{\text{an}} \frac{\partial^\alpha P_s(x,t)}{\partial |x|^\alpha} \ , \tag{13}$$

with an appropriate exponent, (β,α), that can be fractional and with an anomalous diffusion coefficient, D_{an}. Although the second and higher moments of x are infinite for $\beta < 1$ and $\alpha < 2$, space-time truncated moments are finite. Only they are considered in the numerical calculations and in the analytical interpretation of the results. Thus,

$$\langle |x| \rangle \sim t^{\beta/\alpha} \ , \tag{14}$$

with $v = \beta/\alpha$. The ratio, β/α, can be expressed through the scaling parameters, λ_x and λ_t, that characterize the renormalization properties of particle trajectories in space and time, respectively. Namely,[18]

$$v = \ln \lambda_x / \ln \lambda_t \ , \quad (\lambda_x \lambda_t > 1) \ , \tag{15}$$

which follows directly from Eq. (13) after the rescaling of the time and space coordinates

$$x \to \lambda_x x \ , \quad t \to \lambda_t t \ . \tag{16}$$

The most difficult part of the diagnostics of particle dynamics is obtaining the parameters λ_x, λ_t. One possibility is the calculation of the escape time statistics for particles in stochastic jets because only these particles are responsible for the long-term asymptotics of the escape time distribution. Following Ref. 23, consider a domain A of the escaping particles in phase space with a phase volume $\Gamma_0 = \Gamma(A)$. Assume that the particle dynamics are Hamiltonian although the plasma flow is not. Hamiltonian dynamics preserve phase volume Γ_A during the time evolution. but the enveloped coarse-grained

volume Γ_t grows with time. The escaped particles from A are dispersed in the volume Γ_t after time t, and the effective number of particles that occupy Γ_t is

$$n_t \sim t\Gamma_t \ . \tag{17}$$

The corresponding integrated probability of a particle to escape from A during t is

$$P_{\text{int}}(t) \sim t_0\Gamma_0 / t\Gamma_t \ , \tag{18}$$

where t_0 is a characteristic time.

In the two-dimensional (2-D) phase space (x, p_x), we can estimate

$$\Gamma_t \sim xp_x \sim x^2/t \ . \tag{19}$$

Here, p_x is the component of the moment of the tracer particle in the x direction. We can now estimate the escape probability as

$$P_{\text{esc}}(t) = \frac{d}{dt} P_{\text{int}}(t) \sim t_0\Gamma_0 / tx^2 \sim t_0\Gamma_0 / t^{\gamma} \ , \tag{20}$$

with $\gamma = 1 + 2\nu$. In Eq. (20), we have introduced the particle escape probability density $P_{\text{esc}}(t)$ with a corresponding characteristic decay exponent γ.

All of these estimates were for one-dimensional (1-D) trajectories. Real dynamics of tracers in the calculations are 3-D, and all trajectories, determined as jets, are elongated in the toroidal direction. Numerical calculations give a diffusive dispersion of tracers in the radial direction, characterized by an exponent ν $\nu(1) \sim 0.8$. We also calculated the trapping time probability, $P(t)$, (see Fig. 7) that scales as

$$P(t) \sim 1/t^{\gamma_\ell} \ , \tag{21}$$

with $\gamma_\ell \sim 1.83$. It is easy to find a connection between γ_ℓ and γ. Let us consider a tracer that travels inside a jet as a "flight." Assuming that the distribution of the flights along the tube of the length ℓ is approximately uniform and that $\ell \sim \text{const.}\, t$, we conclude that

$$P(t) \sim \ell P_{\text{esc}}(t) \sim t P_{\text{esc}}(t) \ . \tag{22}$$

This result implies that $\gamma_\ell = \gamma - 1 = 2\nu$. Therefore, γ = 1.76±0.14, consistent with the numerical result γ = 1.83±0.22 from Fig. 7.

5. Discussion and Conclusions

We have investigated the transport properties of a 3-D pressure-gradient-driven turbulence. This system was characterized by subcritical transport by avalanches when a noise source was introduced in the equations. Similar properties of avalanche transport are found in the supercritical regime. The use of particle tracers in this system has allowed us to characterize, through different diagnostics, the transport properties of the tracers in such a system.

The main results are that the transport is superdiffusive with a transport exponent of ν = 0.88±0.07. There is no change of the exponent, within the error bars, in going from subcritical to supercritical transport. Several of the methods used in calculating this exponent lead to the same result.

The transport picture coming from these calculations agrees with the one put forward in Ref. 2. Particles are trapped in eddies at the resonant surfaces; they move as jets along the torus. When the particles reach near the boundary of the eddy, where the trajectories become stochastic, they travel fast radially. As they do that, they can travel across several eddies in a single flight. This combination of trapping and flights is consistent with the simple picture given by the sandpile model of Ref. 4.

The transport dynamics of the tracer particles may be interpreted with fractional kinetics. This interpretation provides a consistent picture of the trapping time distributions and the radial anomalous diffusion exponent.

Acknowledgments

One author (BAC) gratefully acknowledges useful discussions with D. E. Newman, Diego del-Castillo-Negrete, and A. Vulpiani. This research is sponsored by the Office of Fusion Energy, U.S. Department of Energy, under contract DE-AC05-00OR22725 with UT-Battelle, LLC, and Cooperative Agreement DE-FC02-99ER54512. Another author (GMZ) was supported by U.S. Navy Grant No. N00014-96-10055 and by the U.S. Department of Energy Grant No. DE-FG02-92-ER54184.

References

[1] Petty

[2] N. Lopez Cardozo, *Plasma Phys. Contr. Fusion* **37**, 799 (1995).

[3] K. Gentle et al Phys. Plasmas

[4] D. E. Newman, B. A. Carreras, P. H. Diamond et al., *Phys. Plasmas* **3**, 1858 (1996).

[5] P. Bak, C. Tang, and K. Wiesenfeld, *Phys. Rev. Lett.* **59**, 381 (1987).

[6] Jensen, Self-Organized criticality, Oxford University Press

[7] H. E. Hurst, *Trans. Am. Soc. Civil Eng.* **116**, 770 (1951).

[8] B. A. Carreras, B. v. Milligen, M. A. Pedrosa *et al*., *Phys, Rev. Lett*. **80**, 4438 (1998)..

[9] B. A. Carreras, B. v. Milligen, M. A. Pedrosa et al., *Phys. Plasmas* **6**, 1885 (1999).

[10] P. Politzer, *Phys. Rev. Lett*.

[11] B. A. Carreras, D. Newman, V. E. Lynch et al., *Phys. Plasmas* **3**, 2903 (1996).

[12] X. Garbet and R. E. Waltz, *Phys. Plasmas* **5**, 2836 (1998).

[13] P. Beyer, et al, *Phys Plasmas* (1998).

[14] L. P. Kadanoff, S. R. Nagel, L. Wu et al., *Phys. Rev. A* **39**, 6524 (1989).

[15] T. Hwa and M. Kadar, *Phys. Rev. A* 45, 7002 (1992).

[16] B. A. Carreras, V. E. Lynch, D. E. Newman, and G. M. Zaslavsky, *Phys. Rev. E* **60**, 4770 (1999).

[17] G. M. Zaslavsky, *Physica D* **76**, 110 (1994); *Chaos* **4**, 25 (1994).

[18] G. M. Zaslavsky, M. Edelman, and B. A. Niyazov, *Chaos* **7**, 159 (1997)

[19] L. Garcia, H. R. Hicks, B. A. Carreras, L. A. Charlton, and J. A. Holmes, *J. Comput. Phys.* **65**, 253 (1986).

[20] J. Doson...

[21] other

[22] R. N. Mantegna and H. E. Stanley, *Phys. Rev. Lett.* 73, 2946 (1994).

[23] V. Artale, G. Boffetta, A. Celani, M. Cencini, and A. Vulpiani, *Phys. Fluids* **9**, 3162 (1997)

[24] V. V. Afanas'ev, R. Z. Sagdeev, and G. M. Zaslavsky, *Chaos* **1**, 143 (1991).

[25] G. M. Zaslavsky and M. Edelman, *Chaos* **11**, 295 (2001).

.

Figure Captions

Fig. 1. Example of two tracer particle orbits having extreme behaviors. One is trapped in an eddy, while the other is doing several flights.

Fig. 2. The n = 1 and n = 2 moments of the tracer particle positions started near r/a = 0.3. A power fit to the asymptotic time scaling of the two moments gives ν = 0.91 and ν = 0.84, respectively.

Fig. 3. The $\nu(n)$ for several moments of the distribution. The plot shows two asymptotic regions, the low-n and high-n regions. They provide information on two regions of the PDF, for low-r and high-r, respectively.

Fig. 4. For the same plasma parameters and initial tracer particle positions as the calculation of Fig. 2, we have plotted the values of the nonlinear Lyapunov number λ as a function of δ for two radial position of the initial tracers.

Fig. 5. In the case of supercritical transport, the plot of $\lambda(\delta)$ versus δ gives an exponent $\nu = 0.89 \pm 0.14$; this value is very close to the ones obtained for subcritical transport.

Fig. 6. PDF of the radial positions where two particles that started close together separate. We have used a requirement of 100 events per bin to minimize noise; therefore, only the structure associated with low rational surfaces remains. In the figure, we have also plotted the positions of these low rational surfaces.

Fig. 7. The PDF of the trapping times of the particle tracers. For the large values of the trapping times, the PDF decays as a power with an exponent $\gamma = -1.83 \pm 0.22$.

Fig. 8. The PDF of the length along the trajectory of the particle tracers. For the large values of the length, the PDF decays as a power with an exponent of –2.08. This may reflect that the toroidal velocity, which is a constant random number, dominates the particle motion along the orbit.

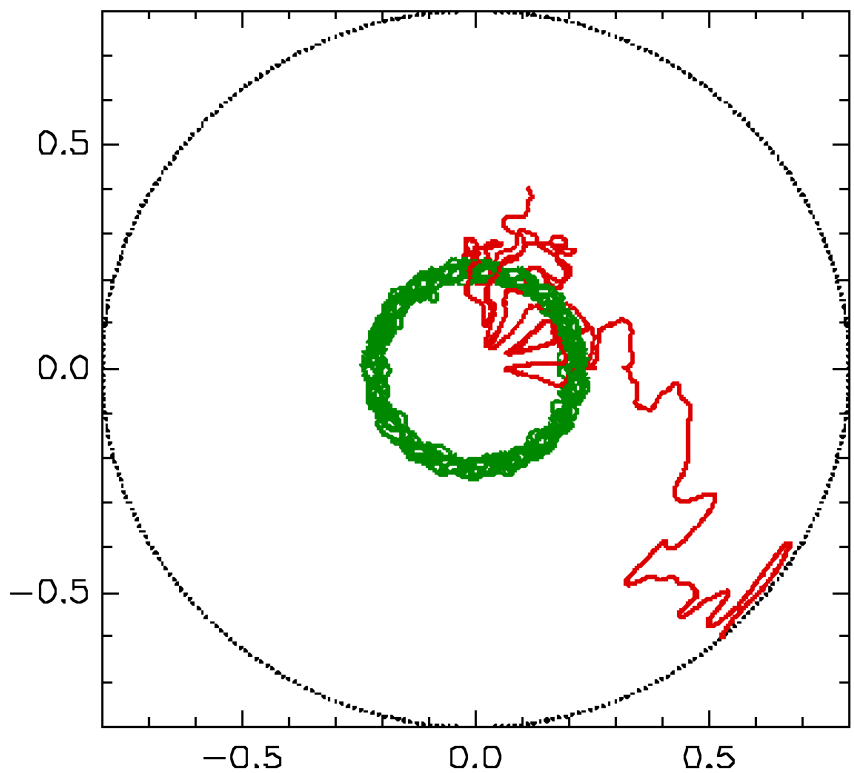

Fig. 1

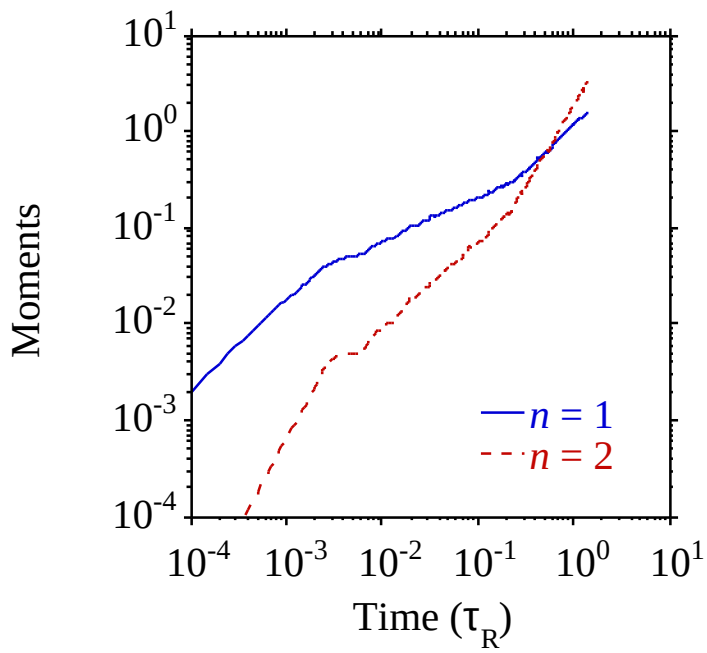

Fig. 2

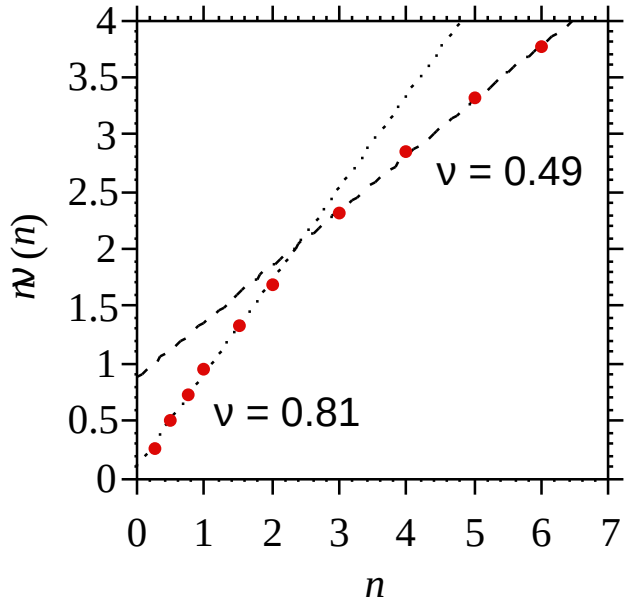

Fig. 3

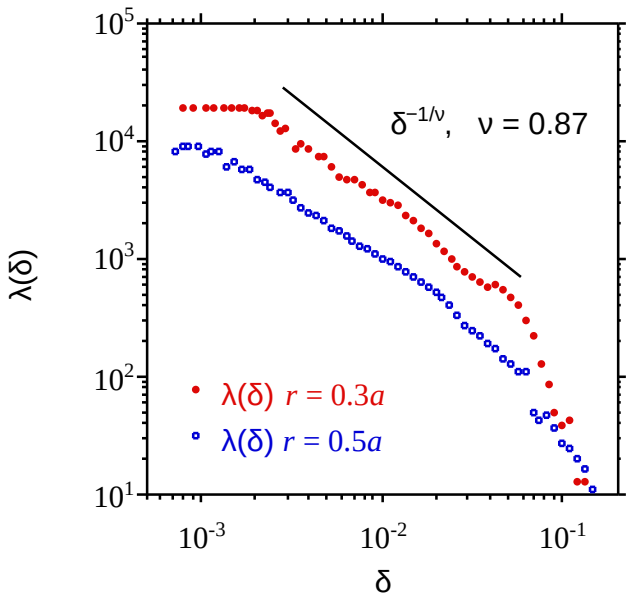

Fig. 4

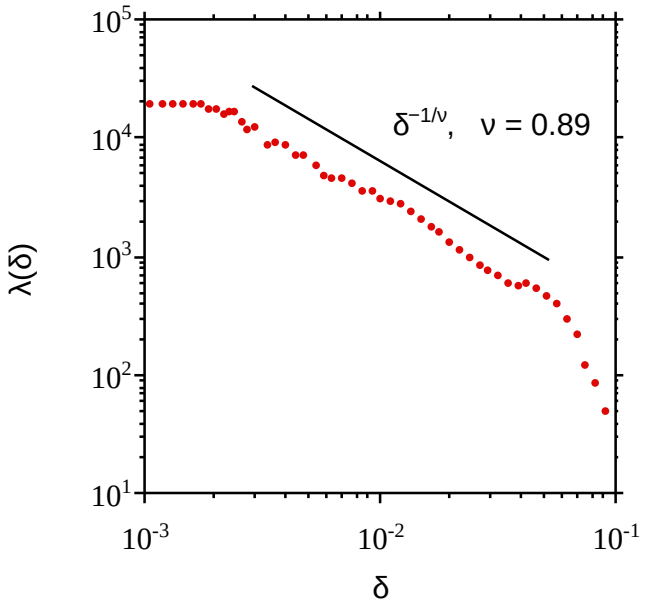
10^5
10^4
10^3
10^2
10^1
λ(δ)
$\delta^{-1/\nu}$, ν = 0.89
10^{-3}
10^{-2}
10^{-1}
δ

Fig. 5

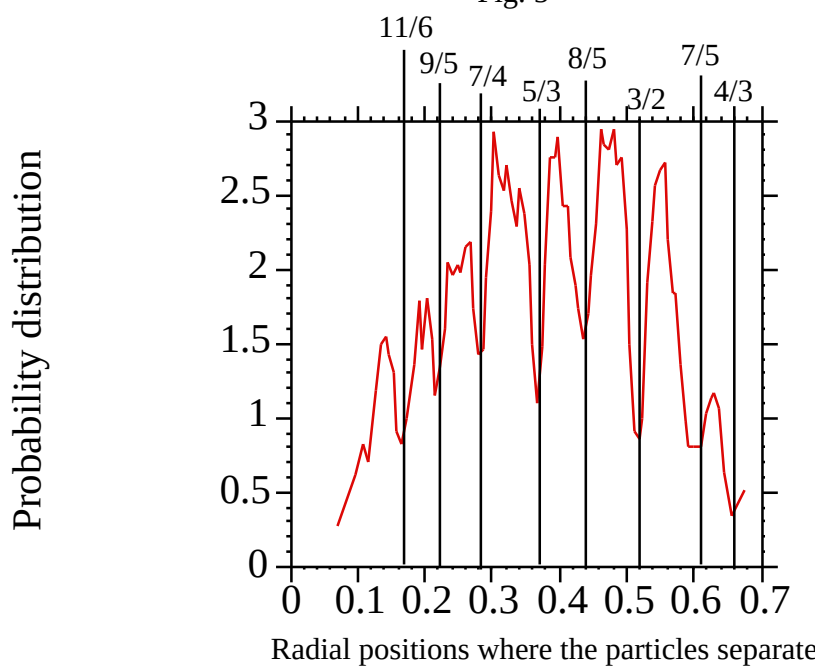
11/6
9/5
7/4
5/3
8/5
3/2
7/5
4/3
Probability distribution
3
2.5
2
1.5
1
0.5
0
0 0.1 0.2 0.3 0.4 0.5 0.6 0.7
Radial positions where the particles separate

Fig. 6

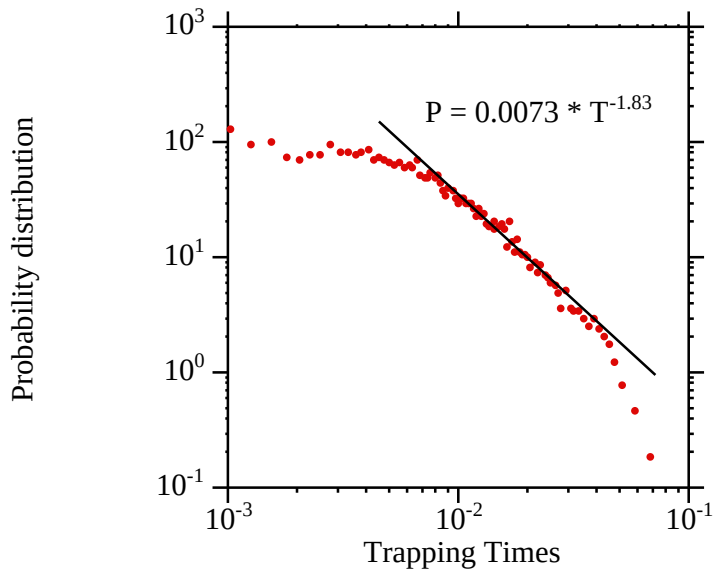
P = 0.0073 * T^-1.83
Probability distribution
Trapping Times
10^3
10^2
10^1
10^0
10^-1
10^-3
10^-2
10^-1

Fig. 7

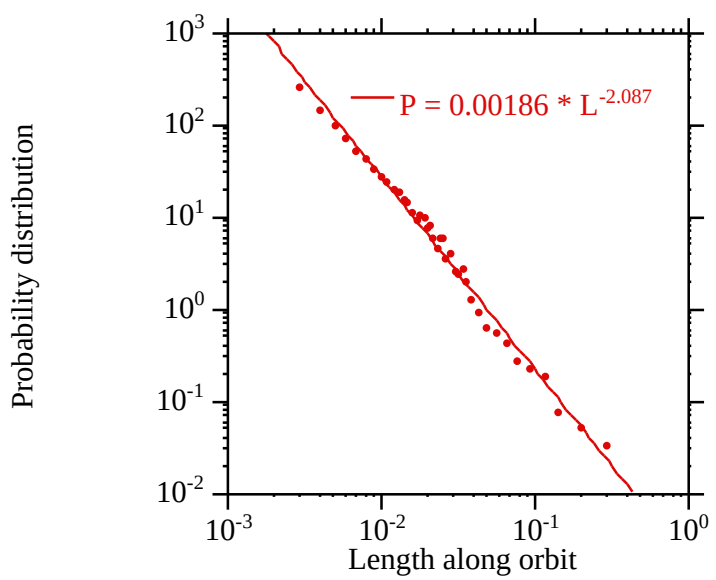
P = 0.00186 * L^-2.087
Probability distribution
Length along orbit
10^3
10^2
10^1
10^0
10^-1
10^-2
10^-3
10^-2
10^-1
10^0

Fig. 8